PHOTOELECTRIC SIGNAL PROCESSING SYSTEM DESIGN BASED ON AUTOMATIC GAIN CONTROL AND ITS APPLICATION

Mengfeng SHEN[1], Ning LI[2*], Tingzhou WANG[3], Zhiyuan SHEN[3]

As a high-precision detection technique, infrared photoelectric detection has been extensively applied across various fields. This study presents an innovative approach to the design and implementation of an infrared photoelectric weft detection system. The working principle of the infrared photoelectric weft detection circuit is thoroughly analyzed, and a digital detection method is proposed, incorporating modulation, demodulation, and adaptive amplification of sensing signals. The developed system integrates three core functionalities: light source driving, sensing signal processing, and MCU-based detection. The signal processing circuit is meticulously designed, comprising a transimpedance amplification circuit, a precision rectifier circuit, and an automatic gain control (AGC) amplification circuit. To enhance signal reliability, sporadic random noise is effectively filtered using a sliding averaging algorithm and a sliding peak-to-peak algorithm, while a threshold detection algorithm is employed for rapid and accurate identification of weft yarn passage signals. Furthermore, anti-interference experiments and real-world operational tests were conducted. The results demonstrate that the proposed infrared photoelectric weft detection circuit significantly reduces false detections caused by occasional interference signals through advanced digital signal processing of the weft passage signal.

Keywords: Infrared Photoelectric; Reliability; Anti-interference; Signal Processing; Noise Factor

1. Introduction

Infrared photoelectric detection is a widely adopted method in high-precision detection applications due to its wide applicability, rapid response, and high resolution [1,2]. Its versatility has been demonstrated in various fields, such as defect detection, real-time monitoring, and industrial automation. Glazzard Martha et al. [3] developed an infrared photoelectric positioning based on clothing defect detector, highlighting its potential in textile quality control. The related literatures [4-6] utilized infrared photoelectric detection to identify surface defects in devices by analyzing image defect coordinates, emphasizing its role in precision engineering. Huang et al. [8] improved detection reliability by incorporating automatic gain modulation, attributing previous limitations to gain and threshold

[1] Hangzhou Polytechnic, 198# Gaoke Rd., Fuyang, Hangzhou, 311402, China
[2*] Hangzhou Dianzi University, Information Engineering College, 1# Hangdian Rd, Lin'an, Hangzhou, 311305, China, corresponding author: lintlt515@126.com
[3] Ningbo Hongda Textile Instrument CO., LTD. 168# Shanshan Rd, Yingzhou, Ningbo, 315000, China

resistance [7]. However, their study was constrained by a small sample size and insufficient consideration of environmental factors, which are critical in real-world applications. Despite its advantages, infrared photoelectric detection systems face challenges such as device aging, light and electromagnetic interference, and significant variations in target size. These factors often introduce large-amplitude sporadic random noises into the detected signals, compromising the reliability and accuracy of the results [9]. To address these issues, advancements in light source-driven circuits and photoelectric signal processing methods are essential.

In this study, we propose a highly reliable infrared photoelectric weft detection circuit based on established photoelectric detection principles [10]. By employing moving average algorithms and moving peak-to-peak algorithms, we effectively filter sporadic random noises, enhancing the system's accuracy and interference resistance. The correlation results show that this testing method can effectively achieve the impact of sporadic interference on the missed detection rate compared to conventional systems. The applied approach not only improves detection reliability but also addresses the limitations of previous studies, and the results can offer a robust solution for industrial applications.

2. Working principles of infrared detection circuit

Fig. 1 illustrates the fundamental principles of infrared photoelectric detection, which play a critical role in modern spinning technology. The detection system is composed of two main components: the optical detection module and the circuit module.

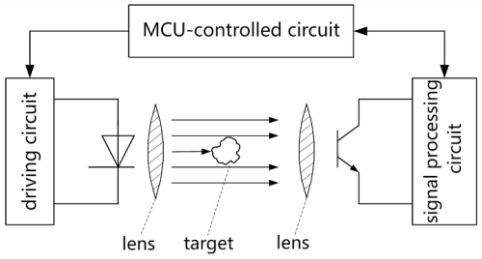

Fig. 1 Working principles of the weft detection circuit

In this study, a near-infrared LED with a concentrated spectral peak and extended service life was selected as the light source, while an infrared phototransistor with inherent amplification capability was employed as the light receiver [11-14]. These components were carefully matched to ensure optimal performance, with both devices operating at a wavelength of 850 nm. Additionally, the infrared filter was incorporated to mitigate ambient light interference, leveraging its selective translucency to enhance signal clarity and reliability.

3. Analysis of weft detection circuit

3.1 Light source-driven circuit

To address the limitation of the long-term stability and reliability of weft detection circuits, a crossflow power source was implemented as the driving power supply for the proposed circuit. This design choice enhances the robustness and durability of the system, ensuring consistent performance under varying conditions. To mitigate broad spectral range and fluctuating intensity effects [15], pulse modulation driving was employed to impart modulation characteristics to the emitted light. This modulated signal, combined with a dedicated signal conditioning circuit for demodulation, allows for the selective reception of the detection light. By filtering out ambient light interference, this method significantly enhances the signal-to-noise ratio (SNR) and ensures precise detection of the target signal [16].

The response time of an infrared phototransistor to light typically ranges within a few microseconds, necessitating a modulation frequency for infrared light that aligns with this characteristic [17]. In this study, the modulation frequency was set to 80 kHz, falling within the optimal range of 50-100 kHz for such applications. This frequency ensures efficient synchronization between the light emission and detection phases, minimizing latency and enhancing system responsiveness. Fig. 2 illustrates the design of the infrared source-driven circuit.

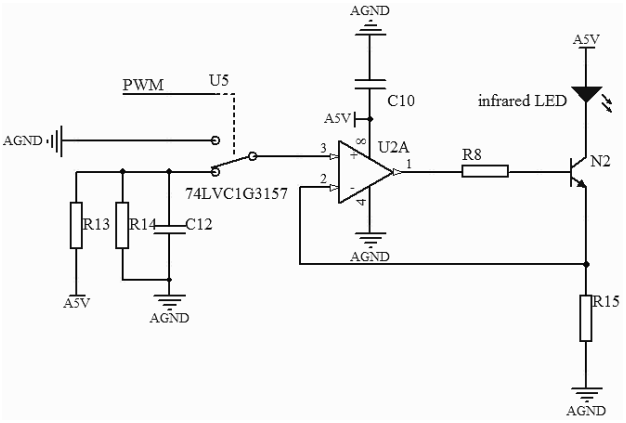

Fig. 2 Light source-driven circuit

The modulation frequency is precisely controlled by pulse-width modulation (PWM) waves generated by the microcontroller unit (MCU). This approach allows for fine-tuned control over the infrared light emission, ensuring stability and accuracy in the detection process [13]. This design not only optimizes the modulation frequency but also ensures the stability and accuracy of the light source, which are critical for reliable detection in applications such as weft detection in textile manufacturing.

3.2 Signal processing circuit

To address the issues of low intensity, susceptibility to attenuation, and significant transmission losses of the photoelectric sensing signals, advanced signal amplification and filtering techniques are indispensable for enhancing the quality and usability of the photoelectric sensing signals. Fig. 3 presents the innovative design of the signal processing circuit, which integrates a multi-stage amplification and filtering architecture. This circuit is specifically engineered to amplify weak photoelectric signals while effectively suppressing noise and interference, thereby ensuring robust signal integrity. The inclusion of adaptive filtering mechanisms further enhances the system's ability to operate reliably in dynamic and noisy environments, a critical requirement for industrial applications such as weft detection in textile manufacturing. The proposed signal processing circuit represents a significant advancement over traditional designs by incorporating precision components and optimized signal conditioning algorithms.

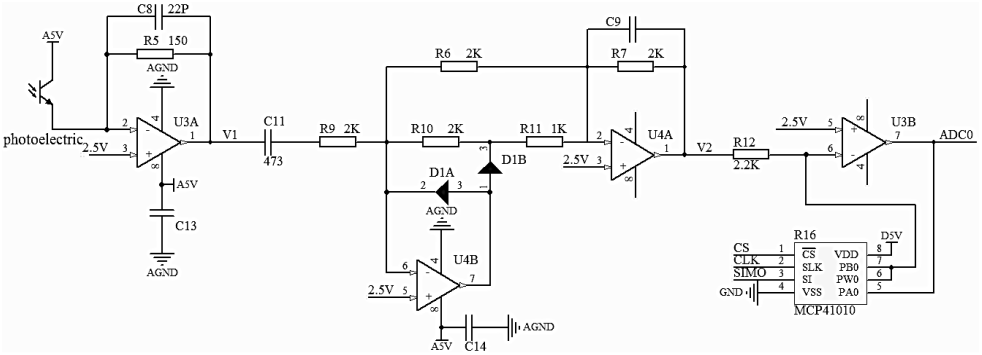

Fig. 3 Signal processing circuit

3.2.1 Transimpedance amplification circuit

The electric signals generated by the infrared phototransistor under light exposure are inherently weak current signals, which are often too small to be measured directly. A transimpedance amplification circuit was employed as the front-end amplification stage. This design not only prevents voltage drops across the measurement circuit but also effectively suppresses signal noise, ensuring high-fidelity signal acquisition [14].

The transimpedance amplification circuit leverages the high input impedance and high gain characteristics of operational amplifiers. The feedback resistor in this circuit determines the gain between the output voltage and the input current, enabling precise signal amplification. For this purpose, the AD823 operational amplifier was selected due to its exceptionally low input bias current (3 pA) and minimal input noise (16 nv/Hz), making it ideal for amplifying weak photoelectric signals with minimal noise introduction. Additionally, the circuit incorporates a low-pass filter composed of a feedback resistor (R5) and a parallel

capacitor (C8), as illustrated in Fig. 3. This filter is specifically designed to attenuate low-frequency noise, further enhancing the signal-to-noise ratio (SNR) and ensuring the accuracy of the processed signals. By integrating these advanced components and design features, the proposed circuit achieves superior noise suppression and signal clarity, which are essential for high-precision infrared photoelectric detection.

3.2.2 Precision rectifier circuit

Despite amplification by the front-end transimpedance circuit, the sensing signals remain in an amplitude-modulated form, necessitating further demodulation to extract the underlying information. To overcome these challenges, this study introduces a precision full-wave rectifier circuit, as depicted in Fig. 3. This circuit utilizes a dual operational amplifier (U4) in conjunction with diodes to achieve high-fidelity rectification. Unlike conventional diode-based rectifiers, the proposed design ensures that input signals are accurately rectified and output regardless of their amplitude, effectively eliminating the drawbacks associated with diode voltage drops. This innovation not only enhances signal fidelity but also improves the overall robustness and reliability of the demodulation process. The precision full-wave rectifier circuit represents a significant advancement over traditional methods, enabling high-precision demodulation of amplitude-modulated signals.

The operation of the precision full-wave rectifier circuit is governed by the relationship between the input voltage and the bias voltage. When the input voltage exceeds the bias voltage, diode D1A is turned off, and diode D1B is turned on. In this state, resistors R9 and R10, along with operational amplifier U4B, form an inverting amplifier with a gain of -1. Simultaneously, resistors R6, R7, and R11, together with operational amplifier U4A, constitute an inverting summing circuit with gains of -1 and -2, respectively. This configuration ensures that the output voltage $V2$ equals the input voltage $V1$, preserving the signal integrity.

Conversely, when the input voltage is lower than the bias voltage, diode D1A is turned on, and diode D1B is turned off. In this scenario, the potentials at the left terminal of R10 and the right terminal of R11 are adjusted to match the bias voltage, effectively preventing current flow through these resistors. Resistors R6 and R7, combined with operational amplifier U4A, form an inverting amplifier with a gain of -1. As a result, the output signal $V2$ becomes symmetric to the input signal $V1$ about the bias voltage, ensuring accurate rectification regardless of the input signal's polarity. This dual-mode operation of the precision full-wave rectifier circuit ensures high-fidelity signal processing by eliminating the voltage drop limitations associated with conventional diode-based rectifiers. The circuit's ability to handle both positive and negative input voltages with minimal distortion makes it particularly suitable for applications requiring precise demodulation of amplitude-modulated signals, such as in infrared photoelectric detection systems.

3.2.3 AGC amplification circuit

Although the processed sensing signals are measurable, further amplification is often necessary to achieve the precision required for micro-measurement applications. Moreover, modern detection systems demand intelligent measurement capabilities, where the measurement range can be dynamically adjusted based on the characteristics of the analyte. To address these requirements, automatic gain control (AGC) circuits are widely utilized in photoelectric detection systems. These circuits ensure optimal signal amplification across varying input conditions, enhancing both accuracy and adaptability. A high-precision and stable digital potentiometer (MCP41010) was integrated into the amplification circuit as a feedback resistor, as illustrated in Fig. 3. This configuration enables the microcontroller unit (MCU) to calculate the appropriate amplification factor based on the quantified voltage of the output signals from the amplification circuit. By dynamically adjusting the resistance of the digital potentiometer via its SPI (Serial Peripheral Interface) interface, the MCU can precisely control the gain of the amplification circuit. This approach allows for real-time tuning of the amplification factor, ensuring optimal signal strength regardless of variations in the input signal amplitude. The proposed method leverages the digital potentiometer's programmability to achieve fine-grained control over the amplification circuit's gain. This innovation not only enhances the system's adaptability to different measurement scenarios but also improves its overall precision and stability. By integrating AGC functionality into the signal processing chain, the system can automatically adjust to varying signal intensities, making it highly suitable for applications requiring high sensitivity and dynamic range, such as infrared photoelectric detection in industrial environments.

3.3 MCU-controlled circuit

MCU is a digital control computing unit for modulation control of the photoelectric detection circuit, automatic gain control, signal sampling and result analysis. Fig. 4 shows the connections of its peripheral circuit and functional pins. A digital signal processor (TMS320F28027) with a working frequency of 60 M was employed as the MCU. Herein, 8-channel enhanced PWM, 16-channel, 12-bit analog-to-digital converter (ADC) and 2-channel SPI were arranged for the MCU, and it can operate under a 3.3 V single supply. Additionally, program writing and online debugging were achieved by using the JTAG interface. After power-on initialization, the EPWM1A pins generate 100-kHz square waves to modulate the infrared LED, high-frequency ADC sampling was executed on the output signals of the signal processing circuit, and the impedance of the feedback resistor (MCP41010) in the AGC circuit was tuned according to the sampling results so that the output voltage was within the detection domain.

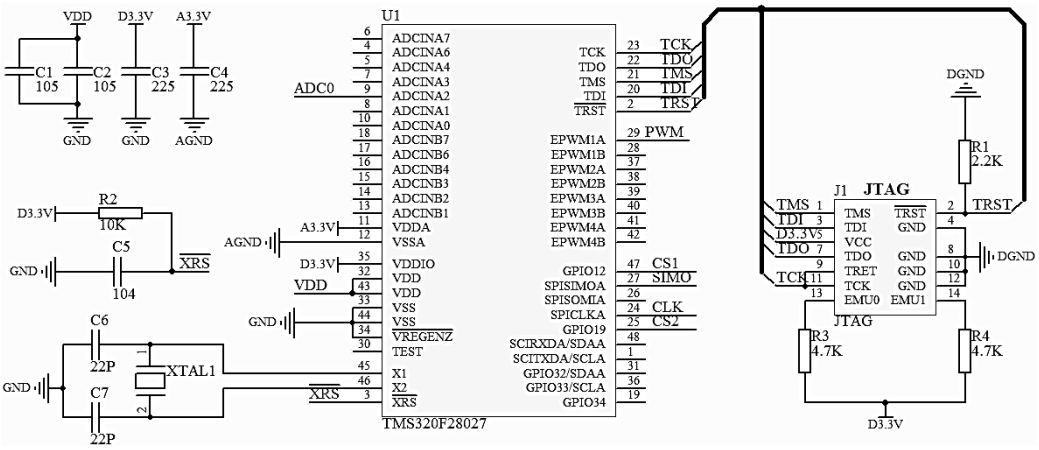

Fig. 4 MCU-controlled circuit

In this way, the measurement results for the analyte can be calculated on the basis of the sampling results the amplification gain and their ratios.

4. Analysis of infrared photoelectric signal processing

4.1 Sporadic peak interference

Time-domain integration of the pulse width and amplitude of the signals revealed that the weft through signals were larger than those of random noises, and the weft through signals comprise both positive and negative signals.

4.2 Analog-to-digital signal conversion

The high-speed collection of the output signals of this amplification circuit was achieved by the ADC in the digital signal processor. The sampling signals were converted from analog signals to discrete digital signals:

$$X(n) = x(nT) \tag{1}$$

where *x(n)* is a time function of signals to be collected; *T* is the sampling interval and equals to the reciprocal of the sampling frequency. The sampling frequency is usually set to be 10 times of that of the signals to be collected to guarantee real-time and precise detection. After detection of the weft through pulse width, the sampling frequency of the ADC was set to be 100 kHz [15-16].

Array recurrent storage sliding processing was employed to tackle the limited storage space of the digital signal processor for discrete signals. Specifically, the discrete signals are processed one-by-one, as shown in Fig. 5. Herein, digital signals collected by the ADC are put into a ‘first-in, first-out’ FIFO array with a fixed width of m according to their emergence sequence, wherein the data in this array is updated in real time for data reading and processing in the program, thereby guaranteeing that the output by the program is real time and accurate.

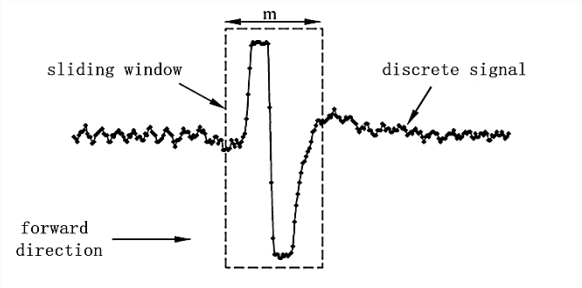

Fig. 5 Moving data processing model

The digital signals comprising weft through signals and random signals can be described by:

$$X(n) = f(n) + e(n) \tag{2}$$

where $f(n)$ refers to the weft through signal and $e(n)$ refers to the random signal.

4.3 Moving average filtering

To effectively suppress the random signal $e(n)$, the digital signals $X(n)$ were processed by using the moving average filtering algorithm, as shown in Eq (3). In this method, the nonstationary signal $X(n)$ in an appropriate period is approximated to be stationary and set as the mean of this period, thereby minimizing the influences by the random signal $e(n)$. Likewise, local averaging of signals in m adjacent periods was executed to eliminate random signals $e(n)$ and obtain the practical weft through signal $f(n)$.

$$Y(n) = \left(X(n-m+1) + X(n-m) + ... + X(n)\right)/m \tag{3}$$

$$\int X(n)d(t) = [X(n-m+1) + X(n-m) + ... + X(n)] * T \tag{4}$$

Time-domain integration of data in these periods is equivalent to local averaging, as illustrated by Eq (4). As indicated, local averaging of the data in these periods can be related to time-domain integration of the data by a coefficient of mT, suggesting that time-domain integration of the data can be reflected by local averaging. Hence, moving average filtering can achieve signals denoising [17].

4.4 Moving peak-to-peak filtering

Analysis of sensing signals after analog filtering in practical weft process revealed that the weft through signal had both positive and negative waveforms (regarded as oscillation), while sporadic random noises had negligible oscillation characteristics. In this study, the amplitude difference of the weft through signals and the sporadic random noises was augmented by extracting the peak-to-peak values of the signals. The signal can be obtained by moving peak-to-peak calculation of the mean output signal $Y(n)$:

$$Z(n) = \max\{Y(n-m+1), Y(n-m), ..., Y(n)\} - \min\{Y(n-m+1), Y(n-m), ..., Y(n)\} \tag{5}$$

4.5 Rapid detection of weft through signal

After moving average filtering and moving peak-to-peak filtering, random noises in the detection signals were effectively removed [18]. Then, weft through incidents shall be counted by using highly real-time detection algorithms, including threshold detection, PID, fuzzy detection, and neural network algorithms. Among them, the PID algorithm outstands by high applicability and real-time adjustment of detection parameters. However, PID is essentially a linear control and would affect the detection accuracy of nonlinear signals; intelligent detection algorithms (e.g., fuzzy detection, neural network) are typically applied in situations with unpredicted system changes and high detection requirements as they have high requirements on the processor performance; the threshold detection algorithm is characterized by real time nature and low requirements on the processor performance, as well as facile setting (only comparison of the physical parameters of the object and the predetermined values is required), and moderate accuracy and applicability. In this study, the threshold detection algorithm was used for detection of weft through signals.

5. Interference resistance

A DC brushless weft storage unit (KT100) was employed in this study. Fig. 6 shows the weft storage unit and water jet loom (JW-851SH, Yinchun, China). A high-resolution oscilloscope (MSO9014A, Agilent) was used for data measurement and recording. The interference resistance of the proposed infrared photoelectric detection circuit was investigated.

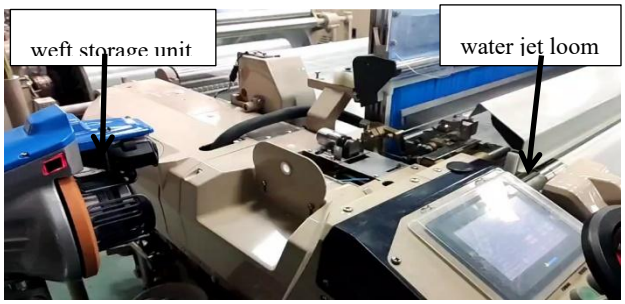

Fig. 6 Weft storage unit and water jet loom

During the operation of the weft storage unit, some yarn may pass through signals with high amplitudes and/or sporadic random noises, and direct utilization of such signals may cause false trigger and missed detection. Hence, such sporadic interference signals were tested.

5.1 Moving average filtering algorithm

Repetitive experiments were conducted with the number of elements in the rolling array (m) being 1, 5, 10, and 20, and the optimal values were selected [19].

In other words, the intensities of interference signals shall be minimized without affecting the effective signals, as shown in Fig. 7. As indicated, the signal-to-noise ratio is improved in all cases, especially at m = 5. The sampling frequency is 50 kHz, wherein the yarn through pulse width is 150 and 200 μs in the positive and negative directions, respectively. When m=5, the rolling number overlaps with the positive pulse width and the negative pulse width is reduced, indicating that the peak information of through signals is effectively retained.

5.2 Moving peak-to-peak filtering algorithm

Repetitive experiments were conducted with the number of elements in the rolling array (m) being 1, 5, 10, and 20, and the optimal values were selected [20]. The results are shown in Fig. 8. The peak information of output signals is extracted by using the moving peak-to-peak filtering algorithm, and the positive and negative components of the yarn through signal are superimposed, thereby improving the signal-to-noise ratio. According to the experimental results, the signal-to-noise ratio is improved in all cases. Therefore, n is set to be 5.

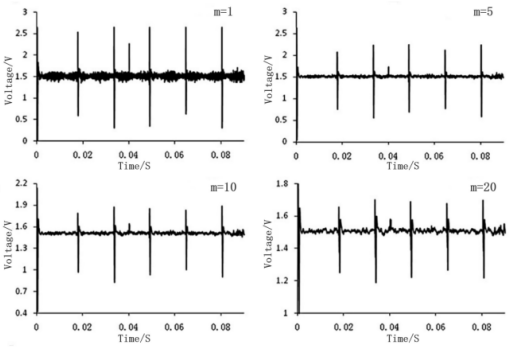

Fig. 7 Results of moving average filtering

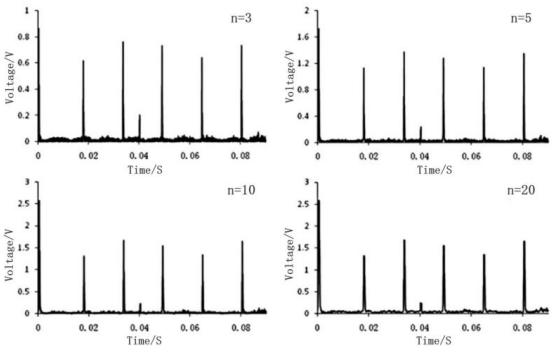

Fig. 8 Results of moving peak-to-peak filtering

5.3 Testing under practical conditions

The proposed detection system was compared with the open-loop constant pressure-driven sensor in 30 d. Herein, daily average count of miss detection, probability of miss detection, daily average count of false detection and noise factor were employed as the indicators [21]. As shown in Table 1:

Table 1

Experimental results by the proposed system and the open-loop constant pressure-driven sensor

Parameter	open-loop constant pressure-driven sensor	proposed infrared phototransistor detection system
Daily average count of miss detection	78	0
Probability of miss detection	0.103‰	0
Daily average count of false detection	31	0.6
Noise factor	0.041‰	0.00079‰

digital signal processing of output signals by the proposed detection circuit led to significantly reduced probability of false detection induced by sporadic interference signals, thereby reducing the noise factor. Compared with the literature [5], it was found that the detection system designed in the research improved the detection efficiency of latitude related parameters of 3 percentage points in the same period.

6. Conclusions

An innovative photoelectric detection circuit was developed, incorporating advanced methodologies such as adaptive amplification, precision rectification, and intelligent noise filtering. These innovations collectively address critical challenges in signal fidelity, dynamic range adaptation, and noise suppression. The proposed circuit demonstrates exceptional detection accuracy and broad applicability, achieving high-fidelity amplification of sensing signals while dynamically adjusting to varying input conditions. By employing a combination of transimpedance amplification, precision full-wave rectification, and automatic gain control (AGC) with a digitally controlled potentiometer, the circuit ensures robust performance in real-world applications. Furthermore, the integration of sliding averaging and peak-to-peak algorithms effectively eliminates sporadic random noises, significantly enhancing signal reliability. The results of the automatic detection and monitoring system designed and applied to the production enterprise show that the system has improved the efficiency of latitude line detection, and solved problems of poor signal fidelity, large noise and low signal reliability in the process of signal acquisition, which meets the needs of the corresponding enterprises.

Acknowledgement: This project was supported by Research topic of the National Industrial and Information Technology Vocational Education Teaching Guidance Committee (GXHZWZ11931), General Research Projects of the Bureau of Education of Zhejiang (Y202043150) and the major/key research plan of the Jinhua Science and Technology Agency (2021-1-061).

REFERENCES

[1] *X.J. Xu, K. E. Kweon, S. Keuleyan, A. Sawvel, E. J. Cho, Ch. Orme.* Infrared photodetectors: Rapid in situ ligand-exchange process used to prepare 3D PbSe nanocrystal superlattice infrared photodetectors, Small, Vol.17, Iss. 25, 2021.

[2] *Q.Y. Wu, Y.J. Liu, X.Y. Huang, X. Zheng, J.Z. He, Z. Ji, W.J. Mai.* Self-powered and broadband germanium/PEDOT: PSS heterojunction photodetectors for near-infrared biomedical imaging applications, Science China. Technological sciences, Vol. 64, Iss. 11, 2021.

[3] *G. Martha, B. Philip.* Weft-knitted auxetic textile design, Physica status solidi B-basic solid-state physics, Vol. 251, Iss. 2, 2014.

[4] *L.Y. Cheng, G.Y. Mi, S. Li, C.M. Wang, X.Y. Hu.* Defects diagnosis in laser brazing using near-infrared signals based on empirical mode decomposition, Optics and laser technology, Vol. 100, 2018.

[5] *C. Kosom, S. Sarun, K. Chakkrit, C. Sataporn.* Optical Sensing System for Real-Time Physical Quality Evaluation of Hand Reeled Silk Yarn, IEEE Journal of Selected Topics in Quantum Electronics, Vol. 27, Iss. 6, 2021.
[6] *K. Le, Y.H. Yuan.* Based on the Geometric Characteristics of Binocular Imaging for Yarn Remaining Detection, Sensors, Vol. 25, Iss. 2, 2025.
[7] *M. Hajjari, N. R. Jafari, T. Dastan, M. Sheikhzadeh, W-R. Yu.* Lightweight weft-knitted tubular lattice composite for energy absorption applications: An experimental and numerical study, international journal of solids and structures, Vol. 213, 2021.
[8] *W.J. Huang, L.Q. Du, T. Yang, H.T. Lin, P.B. Ma.* Integral forming manufacture of weft-knitted 3D hernia repair mesh, Fibers and Polymers, Vol. 24, Iss. 8, 2023.
[9] *A. Serrano, S. Meijer, R. R. van Rijn, S. B. Coban, B. Reissland, E. Hermens, K. J. Batenburg, M. van Bommel.* A non-invasive imaging approach for improved assessments on the construction and the condition of historical knotted-pile carpets, Journal of cultural heritage, Vol. 47, 2021.
[10] *J. Li, Y.X. Wang, W.S. Liang, C. Xiong, W.B. Cai, L.J. Li, Y. Liu.* Visual Anomaly Detection via CNN-BiLSTM Network with Knit Feature Sequence for Floating-Yarn Stacking during the High-Speed Sweater Knitting Process, Electronics, Vol. 13, Iss. 19, 2024.
[11] *H.Q. Chen, J.Y. Lu, K.D. Wang, G.Q. Ding, X. Chen.* Yarn3D-Net: 3D segmentation of wool fabric microstructure using depth-enhanced Swin Transformer and CNN hybrid architecture, Materials Today Communications, Vol. 46, 2025.
[12] *Z.L. Hu, Q. Zhao, J. Wang.* The prediction model of worsted yarn quality based on CNN-GRNN neural network, Neural Computing & Applications, Vol. 31, Iss. 9, 2019.
[13] *S. Gielen, C. Kaiser, F. Verstraeten, J. Kublitski, J. Benduhn, D. Spoltore, P. Verstappen, W. Maes, P. Meredith, A. Armin, K. Vandewal.* Intrinsic detectivity limits of organic near-infrared photodetectors, Advanced materials, Vol. 32, Iss. 47, 2020.
[14] *L.L. Li, H. Xu, Z.X. Li, L.C. Liu, Z. Lou, L.L. Wang.* CMOS-compatible tellurium/silicon ultra-fast near-infrared photodetector, Small, Vol. 19, Iss. 42, 2023.
[15] *C. Pedro, S. Filipe, P. Filipe, L. Helena, M. José.* Automatic system for yarn quality analysis by image processing, Journal of the Brazilian Society of Mechanical Sciences and Engineering, Vol. 44, Iss. 11, 2022.
[16] *Y.S. Tao, F.H. Yang, Z.H. Tao, L. Chang, H.W. Shu, M. Jin, Y. Zhou, Z.F. Ge, X.J. Wang.* Fully on-chip microwave photonic instantaneous frequency measurement system, Laser & photonics reviews, Vol. 16, Iss. 11, 2022.
[17] *S.M. Sim, Y.S. Lee, J.W. Kim, H-L. Kang, I. Llamas-Garro, J-M. Kim.* Frequency discriminator design phase formula with experimental verification for frequency measurement systems with uniform sub-band resolution, International journal of RF and microwave computer-aided engineering, Vol. 31, Iss. 9, 2021.
[18] *R.R. Zhou, P. Poechmueller, Y. Wang.* An analog circuit design and optimization system with rule-guided genetic algorithm, IEEE transactions on computer-aided design of integrated circuits and systems, Vol. 41, Iss. 12, 2022.
[19] *J.M. Du, H.Z. Lu, M.F. Hu, L.P. Zhang, X.L. Shen.* CNN-based infrared dim small target detection algorithm using target-oriented shallow-deep features and effective small anchor, IET image processing, Vol. 15, Iss. 1, 2021.
[20] *L. Zheng, Y.P. Peng, Z.C. Ye, R.Q. Jiang, T.T. Zhou.* Infrared small UAV target detection algorithm based on enhanced adaptive feature pyramid networks, IEEE access, Vol. 10, 2022.
[21] *H. Li, J.Q. Cao, J.L. Chen, X. Liu, Y.W. Shao, Z.Q. Du.* Highly sensitive MXene helical yarn/fabric tactile sensors enabling full scale movement detection of human motions, Advanced electronic materials, Vol. 8, Iss. 4, 2022.